







Three-Dimensional Reconstruction of Enclosed Environments Based on Two-Dimensional LiDAR: Starting Point and Future Challenges

Pablo R. Yanyachi , *Senior Member, IEEE*, Alfredo Mamani-Saico , Flor X. Chacon , Miguel A. Esquivel , Juan Carlos Cutipa-Luque , and Daniel D. Yanyachi 

Abstract—Robotics and LiDAR technology stand as a crucial cornerstone for the development of cutting-edge three-dimensional mapping systems. This study represents a significant advancement by addressing the development of an initial approach for a three-dimensional mapping system, utilizing a unique LiDAR translational mechanism. In pursuit of this objective, a comprehensive review of works exclusively dedicated to mechanisms employing two-dimensional LiDAR has been conducted. This selective approach results in a comprehensive understanding of the mechanism used for three-dimensional reconstruction and lays the groundwork for future endeavors. Furthermore, a robotic prototype has been implemented using the Robot Operating System (ROS), serving as an accessible tool for implementing our initial approach and engaging new researchers from our university in the application of robotics for three-dimensional reconstruction through LiDAR technology. The validation of our study is conducted through tests in both open and closed environments, revealing high data resolution and a correlation of over 98% with the real environment. Despite this good initial result, the current study identifies new challenges to be explored with new prototypes for missions where the attitude is required for robot locomotion.

Link to graphical and video abstracts, and to code: <https://latam.ieceer9.org/index.php/transactions/article/view/8895>

Index Terms—Tridimensional reconstruction; LiDAR; robot operating system; mapping; mobile robots.

I. INTRODUCTION

Light Detection and Ranging (LiDAR) technology utilizes Laser pulses to measure distances and generate point clouds, it provides a comprehensive and precise view of the area of interest. Currently, the accurate representation of enclosed environments is in high demand due to its ability to proactively enhance safety conditions, as in mining [1]. As a result, researchers are focusing on finding the most suitable technique for autonomously collecting data in this context. Despite the invaluable role played by 2D LiDAR technology in map generation [2]–[4], there is limited exploration concerning efficient methodologies for transitioning from 2D cartography

P. R. Yanyachi, A. Mamani-Saico, J. C. Cutipa-Luque, and D. D. Yanyachi are with the Instituto de Investigación Astronómico y Aeroespacial Pedro Paulet, Universidad Nacional de San Agustín de Arequipa, 04000, Arequipa, Peru (e-mails: raulpab@unsa.edu.pe, amamanisai@unsa.edu.pe, jcutipalu@unsa.edu.pe, and dyanyachi@unsa.edu.pe).

F. X. Chacon, and M. A. Esquivel are with the Escuela Profesional de Ingeniería Electrónica, Universidad Nacional de San Agustín de Arequipa, 04000, Arequipa, Peru (e-mails: fchacong@unsa.edu.pe, and mesquivelya@unsa.edu.pe).

to 3D only based on 2D LiDAR. Furthermore, Simultaneous Localization and Mapping (SLAM) is a sophisticated technique widely employed in LiDAR mapping methods. It works by simultaneously creating maps of unknown environments while determining the precise location of a mobile agent within that environment through the integration of sensor data [5]. This advanced technique has been applied to variety of environments, such as mine exploration [6], [7], mapping intricate subway structures [8], aiding in the deployment of rescue robots [9], and several other domains. The following points summarize how the use of 2D LiDAR in SLAM methods meets these challenges:

- *Limited information in the third dimension:* 2D LiDAR sensors capture information in a plane, giving incomplete or inaccurate representation of the 3D environment [1] [10].
- *Mapping problems in dynamic environments:* Combining 2D LiDAR with other sensors can improve the system's ability to detect and track object position changes [11] [12].
- *Odometry Accuracy:* The accuracy of the odometry used in the SLAM method can be affected by vehicle or sensor motion, which can introduce errors into position and orientation estimation [13].
- *Data costs and availability:* Data quality and availability may vary depending on the technology used and the application environment [13] [1].

The purpose of this study is to establish a starting point for the development of future three-dimensional mapping systems using two-dimensional LiDAR data. Let us answer the following questions: What is the current state of three-dimensional reconstruction methods based on 2D LiDAR, what limitations need to be addressed, and how feasible are the proposed solutions to these challenges? Therefore, an initial approach based on a Single-LiDAR Translational mechanism is being evaluated.

This paper is organized as follows: Section 2 provides a comprehensive review of various 3D mapping mechanisms based on 2D LiDAR. Section 3 outlines the initial prototype used in this study. Empirical analysis and presentation of results are detailed in Section 4. Section 5 highlights the significance of this study and outlines potential avenues for further research. Finally, Section 6 summarizes the study's conclusions.

II. RELATED WORKS

In order to comprehend the current state of research regarding three-dimensional point cloud reconstruction techniques, we conducted an exhaustive search of the existing literature, primarily from the last five years. The search was specifically focused on techniques utilizing 2D LiDAR, employing the terms “THREE-DIMENSIONAL,” “RECONSTRUCTION,” and “LiDAR 2D” in titles, abstracts, and keywords in Scopus and IEEE Xplore databases. Seventeen works were selected for a comprehensive analysis of the subject. The Table I summarizes the approach of the selected works.

In the selected works, various types of customized three-dimensional reconstruction systems built from 2D LiDAR devices have been identified. The analysis of some relevant aspects that highlights the approach of each author is presented below.

A. Mapping Mechanism

Analyzing the mapping mechanism reveals a clear classification that encompasses two main approaches: “Multi-LiDAR” and “Single-LiDAR”. The former refers to the simultaneous use of multiple LiDAR 2D devices, each configured to scan specific planes, primarily in the horizontal and vertical directions. The latter mechanism involves the use of a single LiDAR 2D device. Both mapping mechanisms require distinct operating modalities: “Rotational” and “Translational”. The Rotational modality involves the use of stepper motors to rotate the LiDAR as required around the Euler angles, including Yaw, Pitch, and Roll. On the other hand, the Translational modality is characterized by its portability and necessitates an external source of movement to provide odometry information or other position indicators.

On Multi-LiDAR mechanism, Choi *et al.* [16] proposed the use of a portable translational and rotational Multi-LiDAR mechanism up to 50° in the X, Y, and Z directions to obtain three lines intersecting in different planes and to estimate the position based on line-plane correspondences. Similarly, in the study of Wang *et al.* [9] and Memon *et al.* [28], the same mechanism is employed with the motion source being a wheeled mobile robot; in this case, the robot provides the position estimation. On the other hand, Garrido *et al.* [14] employed up to 3 LiDAR devices, adding one at an inclined position to broaden the field of vision and increase point density in plant detection. In all cases, horizontally positioned devices have been used to estimate the position or reference the navigation of the mobile robot.

Recent work has largely employed Single-LiDAR mechanisms. For example, Fang *et al.* [21] present a rotational Single-LiDAR mechanism that consists of two parts: the rotating head and the driving body. The rotating head has a 2D LiDAR that is continuously driven by a stepper motor located in the driving body. Regarding translational Single-LiDAR mechanisms, Hu *et al.* [27] propose a system with a handheld support to collect point clouds from forest areas, while Baek *et al.* [23] use a robotic transportation system with a 15-meter displacement track attached to the robot. Furthermore, their support for three-dimensional reconstruction is grounded

in algorithms and mathematical approaches, which will be analyzed in the following section.

B. Mathematical Foundations

The mathematics used can be classified into three types of studies: For position estimation, three-dimensional projection, and mapping mechanism modeling.

First, position estimation is a process that is used to relate the sensor location to the generated three-dimensional model. Choi *et al.* [16] have developed an algorithm based on a LiDAR system using three line-plane correspondences and were refined by nonlinear optimization. Fang *et al.* [21] describes a parallel motion estimation algorithm and optimizes the global position to convert the mechanism to 6DoF. Another method for estimating the position is using a Kalman filter or its variants [29], this technique can vary depending on the sensors and the mechanism it uses, for example Chen *et al.* [4] describes visual SLAM assisted by IMU that uses an Extended Kalman Filter to achieve a robust and accurate state estimation. Similarly, Hu *et al.* [27] implements a visual-IMU SLAM fusion system based on nonlinear optimization, obtaining a mean square error that is reduced by 4.65% compared to the Kalman filter fusion algorithm. However, position estimation, especially in enclosed environments, is still not reliable due to the complexity of the structure. Li *et al.* [30] have integrated LiDAR-IMU fusion with absolute geographic constraints using UWB anchors through a weakly coupled approach.

Secondly, the study of three-dimensional projection is carried out to find the most efficient method, that is, to optimize the processing time and obtain the highest possible precision in the generated model. In general, the authors have proposed algorithms based on translational and transformational concepts between coordinate systems. For example, in the study by Garrido *et al.* [14], they proposed an equation to reference the scan point with respect to a total station evaluated over time. To do this, they divide the process into two steps: from the total station to the LiDAR sensor and from the LiDAR sensor to the scan point. In a similar way, Hu *et al.* [27] combines the estimated position data with the laser data. This approach allows for projection, densification, and loop closure correction to form a 3D point cloud.

Finally, another way to perform three-dimensional projection is through the mathematical modeling of the mapping mechanism. The works that present this study use static mechanisms, simple mathematical transformations, and do not require motion estimation, since each three-dimensional point is represented in terms of a fixed point. For example, Murcia *et al.* [17] present the kinematic modeling of a rotational Single-LiDAR mechanism and use a calibration algorithm based on the optimization of the model parameters from a reference surface.

C. SLAM Techniques

In unknown enclosed environments, SLAM is essential for dense 3D point cloud reconstruction, GNSS signals are not available, so a robust SLAM technique is necessary to achieve localization, mapping, planning, and control of autonomous

TABLE I
COMPARATIVE SUMMARY OF METHODOLOGICAL APPROACHES BY VARIOUS AUTHORS

| Author | Year | Approach | Applied Mathematics | Main Result |
|---------------------|------|--------------------------------------|--|---|
| Wang [9] | 2014 | Multi-LiDAR Translation | EKF, TF | Creation of a 180 m long digital map |
| Garrido [14] | 2015 | Multi-LiDAR Translation | TF, Translations | Data points distribution: 6.5% Horizontal, 65.8% Vertical, 27.7% Inclined |
| Chen [4] | 2017 | LiDAR Translation | Visual-SLAM, EKF, TF | Computation time cost: 1.098 ms |
| Ocando [15] | 2017 | LiDAR Rotation | - | Generation of a digital Octomap |
| Choi [16] | 2017 | Multi-LiDAR Rotation and Translation | TF, Pose estimation | Construction of a three-dimensional model with 23 planes |
| Murcia [17] | 2018 | LiDAR Rotation | Kinematic model of rotation mechanism | Time cost for rotation: 0.1s to 1s |
| Kang [18] | 2018 | LiDAR Rotation | - | Time cost: 1s, Map resolution: 0.2m per point |
| Zhu [19] | 2018 | LiDAR Translation | Translation model, EKF, Pose and attitude Estimation | Generation of a digital elevation map |
| Prempraneerach [20] | 2018 | LiDAR Rotation with 2 DoF | Rotation mechanism modeling | Creation of a digital model with variable width between 349 and 354 cm |
| Fang [21] | 2018 | LiDAR Rotation | Pose estimation, SLAM | Digital model covering an area of 200m |
| Zhen [22] | 2018 | LiDAR Rotation | - | Achieved optimal mapping speed of 0.5m/s |
| Baek [23] | 2020 | LiDAR Translation | - | Detected changes with a precision of 25 mm |
| Murcia [24] | 2020 | Object Rotation | Kinematic model of rotation mechanism | Conducted Gazebo simulation |
| Oh [25] | 2021 | LiDAR Rotation | - | Creation of a merged digital map |
| Saha [26] | 2021 | LiDAR Translation | - | Model correlation results: Leaf area correlation of 0.9, Slicing approach correlation of 0.44 |
| Hu [27] | 2022 | LiDAR Translation | Pose Estimation, TF, KF | Average relative error: 3.41%, Mean square error against KF: 4.65%, Time cost: 903 μ s |
| Memon [28] | 2022 | Multi-LiDAR Translation | Pose estimation | Creation of merged digital models |

robotic systems [5]. In the selected works, Table I, there are few works that have considered SLAM as a fundamental part of their results. The following Table II details the works that only considered 3D model construction and the works that completed the implementation of the SLAM method, according to the type of mechanism used.

TABLE II
SLAM IMPLEMENTATION IN ENCLOSED ENVIRONMENTS

| Mechanism | Operating modalities | Only 3D map works | SLAM works |
|--------------|----------------------|------------------------------------|------------|
| Multi-LiDAR | Rotational | None | [16] |
| | Translational | [9], [14] | [28] |
| Single-LiDAR | Rotational | [15], [17], [18], [20], [24], [25] | [21] |
| | Translational | [4], [19], [22], [23], [26], [27] | None |

III. INITIAL APPROACH SYSTEM OVERVIEW

This section describes a low-cost, mobile system designed for three-dimensional reconstruction in enclosed environments, as illustrated in Fig. 1. This system represents the starting point for the development of a fully autonomous three-dimensional reconstruction system. It comprises three primary components: scanning, odometry, and reconstruction, which collectively form the hardware and software architecture. Furthermore, this section covers the description of the initial approach of the reconstruction algorithm.

A. Hardware Architecture

Fig. 2 illustrates the layout of the elements comprising the three-dimensional reconstruction system for enclosed environments. Two general blocks are evident: on the right, the CONTROL STATION block consists of a remote computer and a router, through which monitoring occurs and control

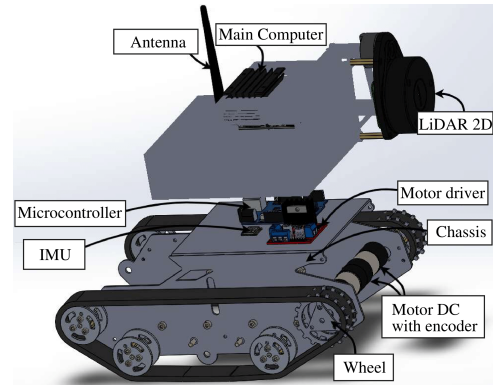


Fig. 1. Mobile robot structure and hardware distribution.

commands are sent to the second block on the left, named ROBOTIC PLATFORM. Within this block are the scanning, odometry, and reconstruction components. The scanning component employs an RPLIDAR A1M8 scanner, the odometry component utilizes encoder, and a microcontroller, while the reconstruction component utilizes an embedded Jetson Nano computer.

Additionally, within the ROBOTIC PLATFORM block, there are actuators and communication elements typical of a mobile robotic platform. Lastly, the figure also displays the communication protocol used by the aforementioned elements.

The system's hardware includes:

- RPLIDAR A1M8 2D LiDAR Device: Tailored for 2D mapping and robotic applications, featuring a 12 m detection range, 0.45° angular resolution, and 8000 samples per second sampling frequency, facilitating high-quality data capture for 3D point cloud generation.
- Jetson Nano: An NVIDIA-developed low-power, small-sized computer serving as the main unit for data pro-

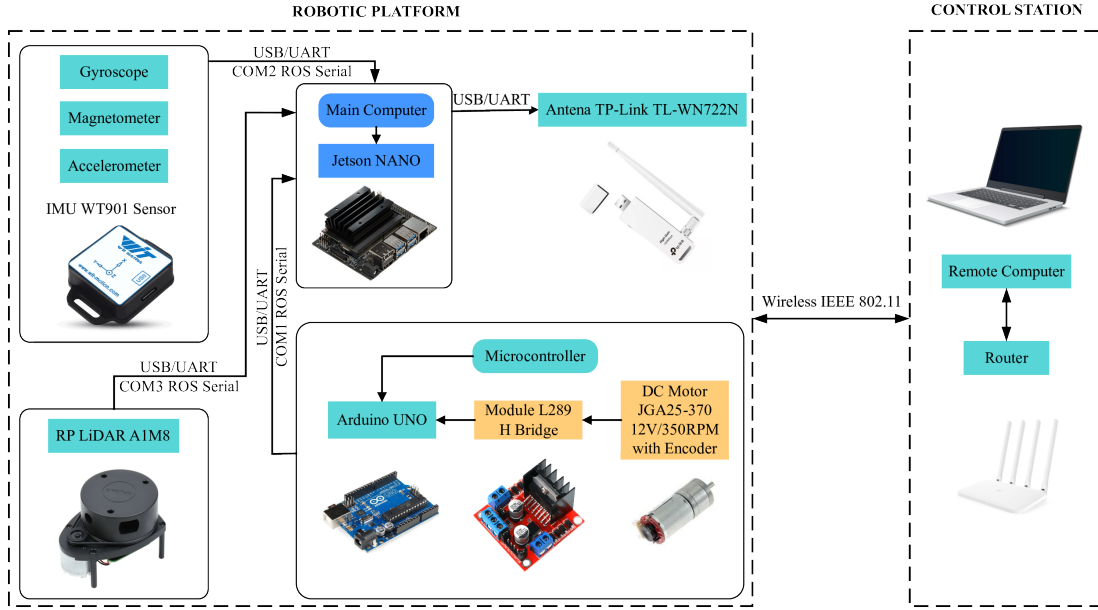


Fig. 2. Hardware architecture for the robotic platform and control station.

cessing and mobile robot control due to its 1.3 GHz processing speed and parallel processing capability.

- WT901C IMU: A sensor providing precise real-time measurements of the robot's orientation, position, and motion via its accelerometer, gyroscope, and magnetometer.
- Arduino UNO Microcontroller, L298n Motor Driver, and Encoder-equipped Motor: Utilized for accurate odometric information by monitoring encoder tick count and employing software algorithms to compensate for slippage or unexpected movements.

B. Software Architecture

The system's software architecture relies significantly on the Robot Operating System (ROS), an open-source middleware software framework tailored for robotics applications, offering tools and libraries to streamline the development of complex robotic systems. In this study, ROS Noetic, an LTS (Long-Term Support) release, was utilized on both the remote and on-board computers. This version ensures stability and compatibility across the system, facilitating seamless integration, communication between devices, and the execution of sophisticated algorithms in the mobile robot setup.

The software architecture comprises four distributed ROS nodes as depicted in Fig. 3. In this setup, the SCAN component is realized through the *rplidarNode*, responsible for laser scanner data acquisition. Conversely, the ODOMETRY component consists of the *ekf_odom_pub* node. Finally, the RECONSTRUCTION component is represented by the *aligned_node* and *constructor_node* nodes, dedicated to point cloud alignment and three-dimensional map construction. The figure details the message types utilized by each node, offering a clear visualization of data interaction and flow among the system components.

C. Three-dimensional Reconstruction Approach

In this section, we delineate the foundational principles guiding the development of forthcoming three-dimensional mapping and location algorithms utilizing 2D LiDAR technology. Fig. 4 outlines the workflow of the process within the RECONSTRUCTION component. The input data consists of variations in the robot's position and the point cloud aligned in a plane. The pose of the robot (x, y, θ) is updated using discrete integration:

$$\begin{bmatrix} x_{k+1} \\ y_{k+1} \\ \theta_{k+1} \end{bmatrix} = \begin{bmatrix} x_k \\ y_k \\ \theta_k \end{bmatrix} + \begin{bmatrix} \Delta t \cdot v_k \cos(\theta_k) \\ \Delta t \cdot v_k \sin(\theta_k) \\ \Delta t \cdot \omega_k \end{bmatrix} \quad (1)$$

where the robot's pose consists of its position (x, y) and orientation θ . Here, v is the linear velocity, ω is the angular velocity, Δt is the time interval between updates and k represent the time step.

Odometry allows estimating the position and orientation of the robot based on the encoder measurements of the wheels. Then, the pose of the robot at can be expressed as:

$$\begin{bmatrix} x_k \\ y_k \\ \theta_k \end{bmatrix} = \begin{bmatrix} x_{k+1} \\ y_{k+1} \\ \theta_{k+1} \end{bmatrix} - \begin{bmatrix} \frac{\Delta s_r + \Delta s_l}{2} \cos(\theta_k) \\ \frac{\Delta s_r + \Delta s_l}{2} \sin(\theta_k) \\ \frac{\Delta s_r - \Delta s_l}{L} \end{bmatrix} \quad (2)$$

where Δs_r and Δs_l are the distances traveled by the right and left wheels, respectively, as measured by the encoders over the time interval Δt . L is the distance between the wheels.

The transformation matrix described in equation 3, where *range* represents the distance measured by the scanner, and *angle* corresponds to the laser beam angle.

$$\begin{bmatrix} x \\ y \\ z \end{bmatrix} = \begin{bmatrix} x_{k+1} - x_k \\ range \times \sin(angle) \\ range \times \cos(angle) \end{bmatrix} \quad (3)$$

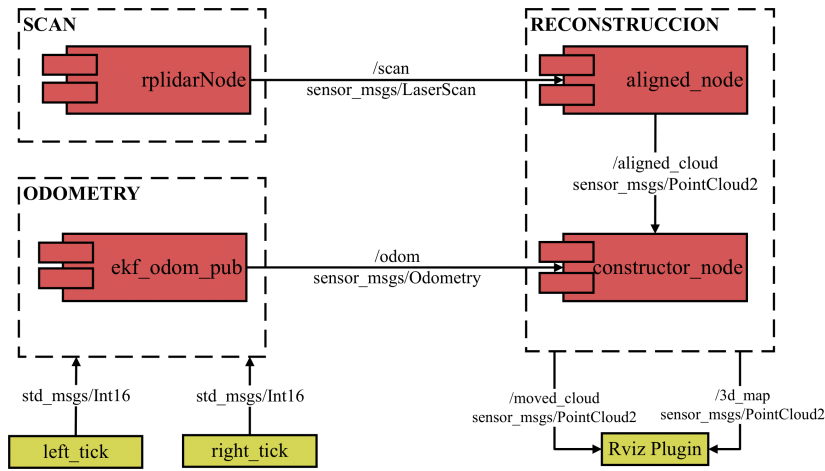


Fig. 3. Software Architecture for the Onboard Computer of the Robotic Platform.

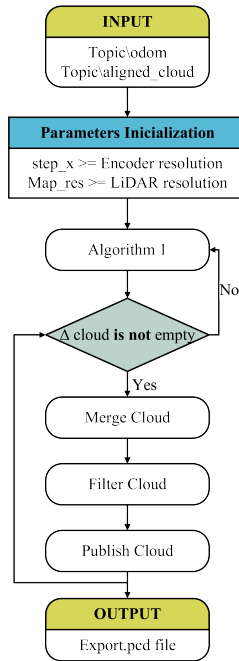


Fig. 4. Data flow.

Algorithm 1 generates a 3D point cloud based on the robot's displacement and encompasses the following input elements 2,4: a vector $pose$ containing information regarding the current position of the mobile robotic platform, and a vector $cloud$ consisting of n elements, representing the quantity of points P_i aligned in the plane YZ .

$$cloud = \{P_{i=1}(x, y, z), P_{i=2}(x, y, z), \dots, P_{i=n}(x, y, z)\} \quad (4)$$

The displacement information along the X axis is added to the x components of each point P_i within the aligned point cloud $cloud$ whenever the position in X reaches the value of $step_x = x_{k+1} - x_k$. The output of the algorithm yields a

new vector structured as follows 5.

$$\Delta cloud = \{P_{i=1}(x_{k+1}, y, z), P_{i=2}(x_{k+2}, y, z), \dots, P_{i=n}(x_{k+n}, y, z)\} \quad (5)$$

Algorithm 1 3D point cloud based on the robot's displacement

Require:

$$cloud = \{P_{i=1}(x, y, z); \dots; P_{i=n}(x, y, z)\},$$

$$pose(x, y, \theta)$$

Ensure:

$$\Delta cloud = \{P_{i=1}(\Delta x, y, z); \dots; P_{i=n}(\Delta x, y, z)\}$$

$$\Delta x_k \leftarrow 0$$

$$\Delta x_{k+1} \leftarrow pose(x)$$

if $|\Delta x_{k+1} - \Delta x_k| \geq step_x$ **then**

for $i = 1$ to $cloud.length$ **do**

$$P_i(x) += \Delta x_{k+1}$$

end for

$$\Delta x_k \leftarrow \Delta x_{k+1}$$

$$\Delta cloud \leftarrow cloud$$

end if

Following the algorithm's validation, non-empty verification of the vector $\Delta cloud$ is performed. Upon satisfying this condition, the point clouds produced by Algorithm 1 are merged. Subsequently, the merged point cloud undergoes filtration via voxelization using the PCL library.

D. Point Cloud Dimensions Validation

To validate the point cloud data with the dimensions of the environment, Pearson correlation is used, since both techniques measure the same physical distance in a controlled and linear environment. The data collected by this correlation were analyzed to quantify the linear relationship between the two series of measurements. To calculate it, the correlation function in Matlab is used, which compares the point cloud data (height and distance between walls) with conventional measurements, following the corresponding formula.

$$r = \frac{\sum_{i=1}^N (x_1 - \bar{x})(y_1 - \bar{y})}{\sqrt{\sum_{i=1}^N (x_1 - \bar{x})^2} \sqrt{\sum_{i=1}^N (y_1 - \bar{y})^2}} \quad (6)$$

where y_1 : is height of the point cloud , x : height of the ceiling, \bar{x} : average height of the point cloud and \bar{y} : average height of the ceiling. They were taken from the data of the distance from the walls in the same way. To evaluate the relative accuracy between the measurements made by the LiDAR sensor and the conventional distance measurements, the bias was calculated in Matlab, using the following formula:

$$Bias = \frac{\sum_{i=1}^N (x_1 - y_1)}{N} \quad (7)$$

IV. EMPIRICAL ANALYSIS AND RESULTS

This study employed two scenarios to assess the performance of the developed system. The first scenario comprises a 2.3 m wide and 7 m long alley with a structure on one side and a room on the other. The presence of a tree next to the room, along with cables and surrounding grass, adds additional features to the environment. This scenario is suitable for evaluating the quality of the point cloud provided by the system in terms of detail level and quantity. Fig. 5 depicts the described scenario along with the relevant characteristics identified in the three-dimensional model.

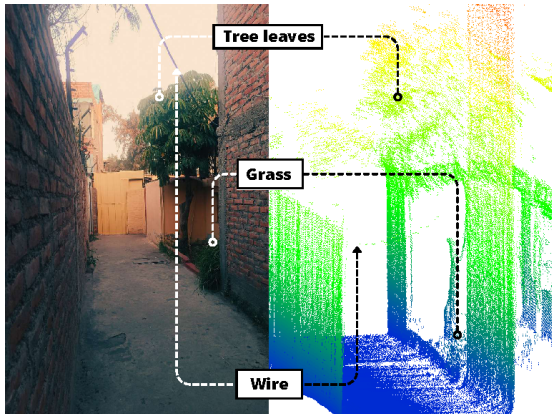


Fig. 5. Relevant characteristics of the first scenario.

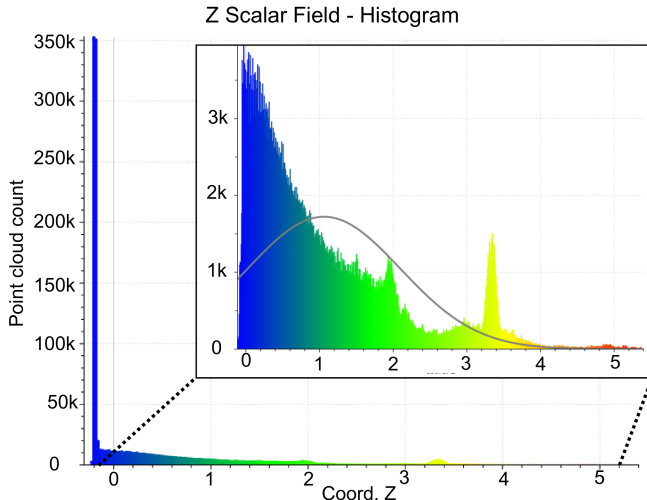


Fig. 6. Gaussian Kernel density curve of the scalar field (axis z) from the survey in an outdoor scenario.

The results of the detail level analysis are presented in Fig. 6. In this figure, the prototype system has provided information from 1,397,678 points, with the majority of points concentrated in the lower part. This occurs due to the inherent characteristics of the environment and the LiDAR's range limitations, where a greater scanning distance results in increased spacing between points.

The second scenario is a fully enclosed rectangular garage, chosen due to its lack of complex objects and regular walls, making it an appropriate environment for cartographic resolution comparisons. Fig. 7 illustrates the obtained results while varying the mapping resolution. In Fig. 7a, the experimental platform is shown in action, capturing measurements of the described scenario. Fig. 7b presents the generated model for a resolution set at 10 centimeters, Fig. 7c at 5 centimeters resolution, and Fig. 7d at 1 centimeter resolution. Table III summarizes the differences between mapping resolutions.

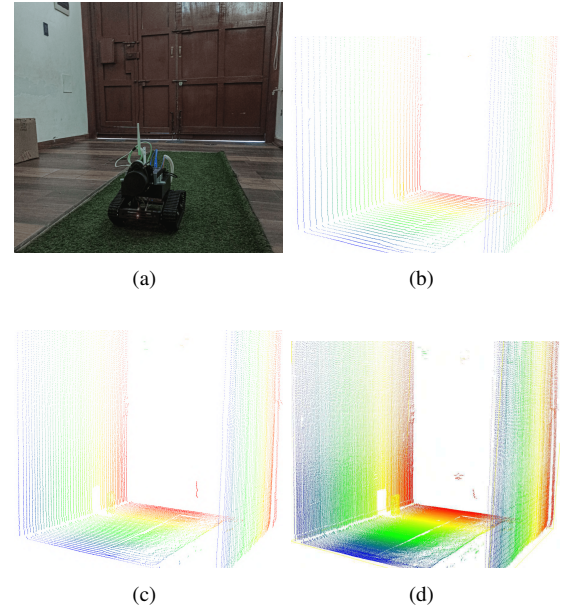


Fig. 7. Three-dimensional model survey with different resolution parameters: (a) Test scenario photograph; (b) Mapping resolution $step_x = 10cm$; (c) Mapping resolution $step_x = 5cm$; (d) Mapping resolution $step_x = 1cm$.

TABLE III
COMPARISON OF THE MODEL AT DIFFERENT MAPPING RESOLUTIONS

| Parameter $step_x$ | Points quantity | Figure |
|--------------------|-----------------|--------|
| 10 cm | 38,592 points | 7b |
| 5 cm | 90,883 points | 7c |
| 1 cm | 430,808 points | 7d |

Furthermore, to ensure the credibility of the acquired data, measurements were carried out in the second scenario employing a high-precision commercial laser meter boasting a resolution of $\pm 1.5mm$. These measurements were then compared with the data derived from the three-dimensional model presented in Fig. 7b, which illustrates the model at a resolution of 10 centimeters. In Fig. 8, the experimental setup employed for distance measurements is illustrated. This includes physical

measurements of height and width, as shown in Fig. 8a, and measurements from the three-dimensional model generated by the prototype system, as depicted in Fig. 8b. In both cases, height and width measurements were taken at 10 cm intervals along a total length of 3 m. The objective is to assess and compare the correlation between these two sets of distance data.

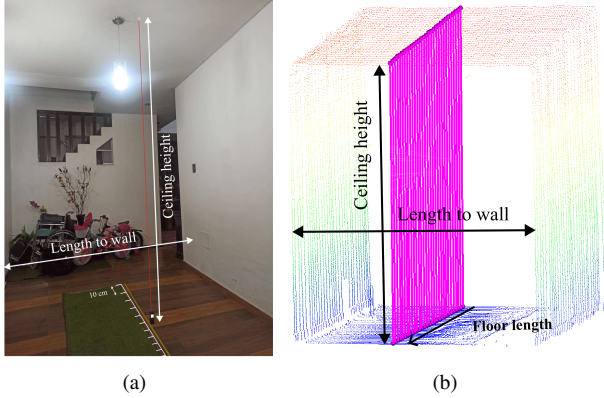


Fig. 8. Experimental setup for measurement comparison: (a) setup for obtaining measurements with the laser meter; (b) software configuration for obtaining measurements from the generated three-dimensional model.

Fig. 9, the measurements of the ceiling height in relation to the floor length in the study environment are presented. These measurements originate both from originate measurements (represented in blue) and from the three-dimensional model generated by the prototype system (represented in magenta). The correlation coefficient between the conventional measurements and the model measurements is 0.9950, indicating a strong correlation, in turn the bias of the data set is -0.0206, being the data collected by the sensor are greater than the data measured originate.

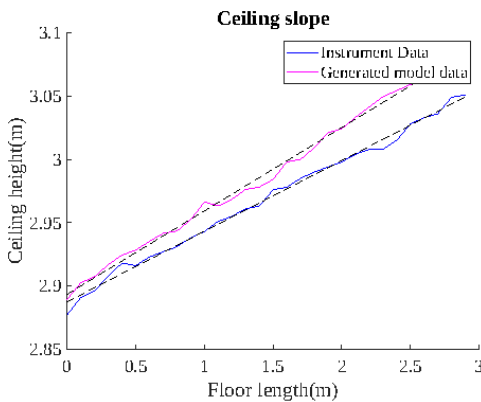


Fig. 9. Height data comparison.

For the length up to the wall of the environment, illustrated in the Fig. 10, the correlation between both sets of data is 0.9888 and the bias obtained is -0.0145, the data obtained by the model being larger than the conventional measurements. However, graphically it is observed that the measurements of the generated model decrease more quickly, coming to intersect with the measurements of the physical instrument.

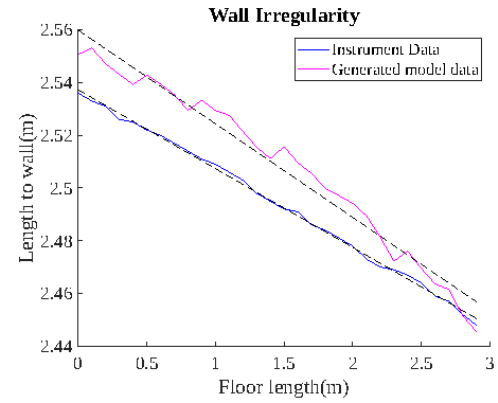


Fig. 10. Width data comparison.

Systematic differences (bias) and linear relationship (correlation) between LiDAR sensor measurements and conventional measurements can be explained by factors such as systematic errors, inherent variability, noise in the data and equipment limitations

V. DISCUSSION OF THE RESEARCH AND FUTURE WORKS

According to Table I, five translational single-LiDAR mechanisms, similar to ours, were identified. Each uses a distinct scanning method, detailed in Table IV. Baek's study analyzes precision with a 3D LiDAR in a precise straight-line scenario. This study, however, shows slightly higher precision in the robot's natural straight-line movement, accounting for vibrations from mechanical construction like wheels and LiDAR mounts.

TABLE IV
COMPARISON SINGLE-LIDAR TRANSLATIONAL METHOD

| Work | Pose source | Model | Accuracy |
|------|------------------------|-------|--|
| [4] | Visual odometry | ✓ | - |
| [19] | UAV position | ✓ | - |
| [23] | Robot position | ✓ | Detection of changes greater than 25 mm |
| [26] | Linear conveyor system | ✓ | Correlation of 0.99 between actual height and estimated height |
| [27] | Visual-IMU odometry | ✓ | Accuracy max: 96.34 % |
| Our | Robot Position | ✓ | Correlation: 0.98 between real scenario and digital model |

Fig. 11 illustrates various attitude configurations of a robotic platform, outlining the scope of the initial approach and identifying challenges that remain to be addressed in future endeavors. The methodology employed in the proposed initial approach is tailored to the configurations depicted in Figs. 11a and 11b, where the 2D LiDAR can only move in a straight line or rotate in the ROLL direction. Meanwhile, Figs. 11c and 11d represent changes in YAW and PITCH orientation that may occur when the robot navigates a real unknown enclosed environment, aspects not covered in any robotic translation mechanism.

To address these challenges, it is suggested to develop a mathematical model of the robot to implement robust odometry based on Inertial Navigation Systems (INS), as referenced

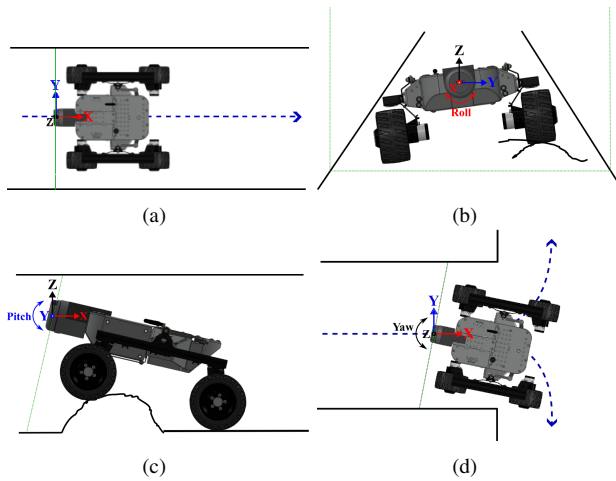


Fig. 11. Robot attitude for mapping: (a) LiDAR scanning in a straight line; (b) LiDAR scanning with Roll angle orientation changes; (c) LiDAR scanning with Pitch angle orientation changes; (d) LiDAR scanning with Yaw angle orientation changes.

in [31]. For the digital model, a robust transformation matrix should be developed using data from an Inertial Measurement Unit (IMU). On the other hand, implementing computational resources for an autonomous system covering large areas presents a challenge. Correcting attitude changes with additional sensors requires a robust odometry estimator and higher resolution LiDARs. Although high-performance onboard computers are becoming more accessible in Latin America, we propose software improvements such as the Data Distribution System (DDS). ROS2 utilizes DDS for robotics, allowing a Linux-based control station to process complex data, leaving the onboard computer to manage only information exchange, such as [32]. This would make the current onboard computer sufficient.

Furthermore, Fig. 12 presents a tentative block diagram for future research. This diagram consists of four stages: data collection, data conditioning, data processing, and desired outputs, with emphasis on the SLAM block in the data processing stage.

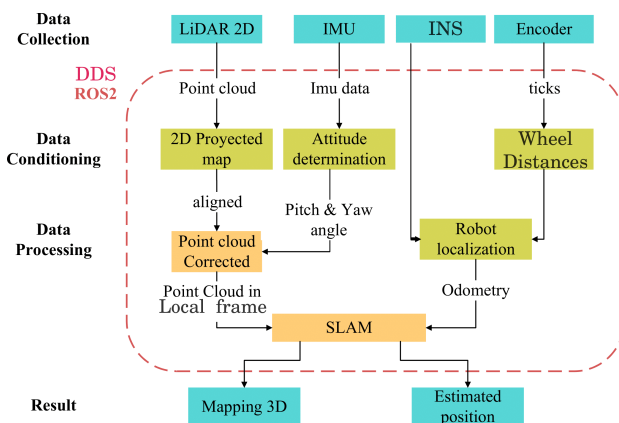


Fig. 12. Block diagram to build ROS package with IMU data.

VI. CONCLUSIONS

This research work has identified the starting point to address future challenges in three-dimensional reconstruction using a Single-LiDAR translational mechanism. A review of related works revealed scarce instances where SLAM techniques have been efficiently developed for such mechanisms. The viability of advancing to the next stage is justified by its potential as a cost-effective and autonomous alternative. It is proposed to implement position estimation based on odometry using Inertial Navigation Systems (INS), develop a robust transformation matrix using an Inertial Measurement Unit (IMU), and address computational resource challenges by improving software through the Data Distribution System (DDS) architecture, such as ROS2.

Additionally, this study presents an initial experimental prototype that implements an algorithm based on the straight-line movement of a robot. Regarding accuracy measurement, a correlation of 99.50% was achieved between conventionally obtained laser measurements and the digital model data for height measurements. Similarly, for width measurements in the second scenario, a correlation of 98.88% was reached, both considering errors caused by platform vibrations. Since this study uses an initial prototype with basic navigation elements and low-cost, short-range LiDAR, it has not been possible to test in larger and multi-directional scenarios.

ACKNOWLEDGMENTS

The authors would like to express their gratitude for the support provided by the Pedro Paulet Institute for Astronomical and Aerospace Research (IAAPP), CAPDS and the Laboratory of Complex Process Control and Unmanned Vehicles, all affiliated with the Universidad Nacional de San Agustín de Arequipa.

REFERENCES

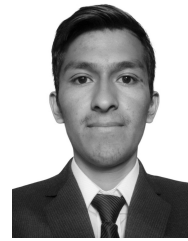
- [1] F. Inostroza, I. Parra-Tsunekawa, and J. Ruiz-del Solar, "Robust localization for underground mining vehicles: An application in a room and pillar mine," *Sensors*, vol. 23, no. 19, 2023.
- [2] L. Yan, J. Dai, Y. Zhao, and C. Chen, "Real-time 3d mapping in complex environments using a spinning actuated lidar system," *Remote Sensing*, vol. 15, no. 4, 2023.
- [3] S. W. Zheng Fang, Shibo Zhao and Y. Zhang, "A real-time 3d perception and reconstruction system based on a 2d laser scanner," *Journal of Sensors*, vol. 2018, p. 14, 2018.
- [4] M. Chen, S. Yang, X. Yi, and D. Wu, "Real-time 3d mapping using a 2d laser scanner and imu-aided visual slam," in *2017 IEEE International Conference on Real-time Computing and Robotics (RCAR)*, pp. 297–302, 2017.
- [5] S. Zheng, J. Wang, C. Rizos, W. Ding, and A. El-Mowafy, "Simultaneous localization and mapping (slam) for autonomous driving: Concept and analysis," *Remote Sensing*, vol. 15, no. 4, 2023.
- [6] X. Zhou, G. Zhao, R. Zhao, Y. Cheng, and Y. Wang, "Mechanism design of a small mobile robot for inspection of underground cables-in-pipe," *Journal of Physics: Conference Series*, vol. 1639, p. 012033, oct 2020.
- [7] J. Martz, W. Al-Sabban, and R. N. Smith, "Survey of unmanned subterranean exploration, navigation, and localisation," *IET Cyber-systems and Robotics*, vol. 2, no. 1, p. 1 – 13, 2020.
- [8] B. Zhou, M. Du, Z. Chen, Y. Liu, Y. Zhang, and Y. Wang, "Design and implementation of intelligent security robot based on lidar and vision fusion*," *Journal of Physics: Conference Series*, vol. 2216, p. 012013, mar 2022.
- [9] Y.-k. Wang, J. Huo, and X.-s. Wang, "A real-time robotic indoor 3d mapping system using dual 2d laser range finders," in *Proceedings of the 33rd Chinese Control Conference*, pp. 8542–8546, 2014.

- [10] P. Prempraneerach and T. Usupan, "Stabilized and rotating mechanism of 2d laser scanner for 3d point cloud reconstruction," in *2018 International Electrical Engineering Congress (iEECON)*, pp. 1–4, 2018.
- [11] X. Xu, L. Zhang, J. Yang, C. Cao, W. Wang, Y. Ran, Z. Tan, and M. Luo, "A review of multi-sensor fusion slam systems based on 3d lidar," *Remote Sensing*, vol. 14, no. 12, 2022.
- [12] L. Yang, H. Ma, Z. Nie, H. Zhang, Z. Wang, and C. Wang, "3d lidar point cloud registration based on imu preintegration in coal mine roadways," *Sensors*, vol. 23, no. 7, 2023.
- [13] Y. Chen, J. Tang, C. Jiang, L. Zhu, M. Lehtomäki, H. Kaartinen, R. Kaijaluoto, Y. Wang, J. Hyyppä, H. Hyyppä, H. Zhou, L. Pei, and R. Chen, "The accuracy comparison of three simultaneous localization and mapping (slam)-based indoor mapping technologies," *Sensors*, vol. 18, no. 10, 2018.
- [14] M. Garrido, D. S. Paraforos, D. Reiser, M. Vázquez Arellano, H. W. Griepentrog, and C. Valero, "3d maize plant reconstruction based on georeferenced overlapping lidar point clouds," *Remote Sensing*, vol. 7, no. 12, pp. 17077–17096, 2015.
- [15] M. G. Ocando, N. Certad, S. Alvarado, and A. Terrones, "Autonomous 2d slam and 3d mapping of an environment using a single 2d lidar and ros," in *2017 Latin American Robotics Symposium (LARS) and 2017 Brazilian Symposium on Robotics (SBR)*, pp. 1–6, 2017.
- [16] D.-G. Choi, Y. Bok, J.-S. Kim, I. Shim, and I. S. Kweon, "Structure-from-motion in 3d space using 2d lidars," *Sensors*, vol. 17, no. 2, 2017.
- [17] H. F. Murcia, M. F. Monroy, and L. F. Mora, "3d scene reconstruction based on a 2d moving lidar," in *Applied Informatics*, (Cham), pp. 295–308, Springer International Publishing, 2018.
- [18] X. Kang, S. Yin, and Y. Fen, "3d reconstruction & assessment framework based on affordable 2d lidar," in *2018 IEEE/ASME International Conference on Advanced Intelligent Mechatronics (AIM)*, pp. 292–297, 2018.
- [19] H. Zhu, H. Wang, and S. Sun, "Research on dem reconstruction based on airborne 2d laser radar," in *2018 37th Chinese Control Conference (CCC)*, pp. 8435–8440, 2018.
- [20] P. Prempraneerach and T. Usupan, "Stabilized and rotating mechanism of 2d laser scanner for 3d point cloud reconstruction," in *2018 International Electrical Engineering Congress (iEECON)*, pp. 1–4, 2018.
- [21] Z. Fang, S. Zhao, S. Wen, and Y. Zhang, "A real-time 3d perception and reconstruction system based on a 2d laser scanner," *Journal of Sensors*, vol. 2018, p. 14, 2018. Article ID 2937694.
- [22] W. Zhen and S. Scherer, "A unified 3d mapping framework using a 3d or 2d lidar," *arXiv e-prints*, p. arXiv:1810.12515, Oct. 2018.
- [23] J. Baek, "Two-dimensional lidar sensor-based three-dimensional point cloud modeling method for identification of anomalies inside tube structures for future hypersonic transportation," *Sensors*, vol. 20, no. 24, 2020.
- [24] H. F. Murcia, D. A. Sanabria, Dehydro-Méndez, and M. G. Forero, "Development of a simulation tool for 3d plant modeling based on 2d lidar sensor," in *2020 Virtual Symposium in Plant Omics Sciences (OMICAS)*, pp. 1–6, 2020.
- [25] S. Oh and S.-Y. Park, "High-density 3d reconstruction in a large space using single camera and 2d lidar," in *2021 International Conference on Computational Science and Computational Intelligence (CSCI)*, pp. 1748–1749, 2021.
- [26] K. K. Saha, C. Weltzien, and M. Zude-Sasse, "Non-destructive leaf area estimation of tomato using mobile lidar laser scanner," in *2021 IEEE International Workshop on Metrology for Agriculture and Forestry (MetroAgriFor)*, pp. 187–191, 2021.
- [27] C. Hu, C. Yang, K. Li, and J. Zhang, "A forest point cloud real-time reconstruction method with single-line lidar based on visual-imu fusion," *Applied Sciences*, vol. 12, no. 9, 2022.
- [28] E. A. A. Memon, S. R. U. N. Jafri, and S. M. U. Ali, "A rover team based 3d map building using low cost 2d laser scanners," *IEEE Access*, vol. 10, pp. 1790–1801, 2022.
- [29] G. Ligorio and A. M. Sabatini, "Extended kalman filter-based methods for pose estimation using visual, inertial and magnetic sensors: Comparative analysis and performance evaluation," *Sensors*, vol. 13, no. 2, pp. 1919–1941, 2013.
- [30] M. Li, K. Hu, Y. Liu, E. Hu, C. Tang, H. Zhu, and G. Zhou, "A multimodal robust simultaneous localization and mapping approach driven by geodesic coordinates for coal mine mobile robots," *Remote Sensing*, vol. 15, no. 21, 2023.
- [31] J. Mendoza-Chok, J. C. C. Luque, N. F. Salas-Cueva, D. Yanyachi, and P. R. Yanyachi, "Hybrid control architecture of an unmanned surface vehicle used for water quality monitoring," *IEEE Access*, vol. 10, pp. 112789–112798, 2022.

- [32] A. Mamani-Saico and P. R. Yanyachi, "Implementation and performance study of the micro-ros/ros2 framework to algorithm design for attitude determination and control system," *IEEE Access*, vol. 11, pp. 128451–128460, 2023.



Pablo R. Yanyachi Doctor in Electrical Engineering-Polytechnic School of the University of São Paulo-Brazil, Master of Science in Automatic Control-Polytechnic Institute of Leningrad. Main Professor of the Academic Department of Electronic Engineering of the National University of San Agustín-Arequipa-UNSA. Station Manager Nasa Laser Tracking Station TLR3-3 in Arequipa - Peru. Director of the Instituto de Investigación Astronómica y Aeroespacial Pedro Paulet (IAAPP - UNSA).



Alfredo Mamani Saico was born in Cusco, Peru, in 2000. He is a senior student of Electronic Engineering at the Universidad Nacional de San Agustín de Arequipa (UNSA). He is currently a junior researcher at the Pedro Paulet Astronomical and Aerospace Institute (IAAPP), UNSA. His research interests are robotics, distributed systems and remote sensing. He has programmed the algorithm presented in this work.



Flor Xiomara Chacon Guillen was born in Arequipa, Peru. She received a B.Sc. degree in Industrial Engineering and a B.Sc. degree in Electronic Engineering from the National University of San Agustín de Arequipa (UNSA). She was a junior researcher at the Pedro Paulet Astronomical and Aerospace Institute (IAAPP), UNSA. Currently, her interests include robotics, autonomous vehicles, industrial instrumentation, and process control.



Miguel Angel Esquivel Yanque was born in Arequipa, Peru, in 1999. He is a senior student of Electronic Engineering at the Universidad Nacional de San Agustín de Arequipa (UNSA). He is currently a junior researcher at the Institute of Astronomy and Aeronautics (IAAPP), UNSA. His research interests include robotics, embedded systems, and advanced control systems.



Juan Carlos Cutipa Luque was born in Arequipa, Peru. He graduated in electronic engineering from the Universidad Nacional de San Agustín de Arequipa, Peru, in 2004, and was granted his M.Sc. and Ph.D. degrees in mechanical engineering from the University of São Paulo, Brazil, in 2007 and 2012, respectively. He is currently a Professor with the Electronic Engineering Department, Universidad Nacional de San Agustín de Arequipa, Peru. His research interests include advanced control systems for autonomous underwater vehicles (AUVs), remote-operated submersible vehicles (ROVs), unmanned surface vehicles (USV), and electric vehicles.



Daniel Yanyachi was born in Peru. He graduated in electrical engineering, with M.Sc. and Ph.D., from the Leningrad Polytechnic Institute. He has lectured for many years as a Full Professor with the Electronic Engineering Department, Universidad Nacional de San Agustín de Arequipa, Peru. His research interests include processing control systems, mining, manufacturing, and complex and advanced control systems.